RSC Advances

ROYAL SOCIETY OF CHEMISTRY

www.rsc.org/advances

Graphical Abstract

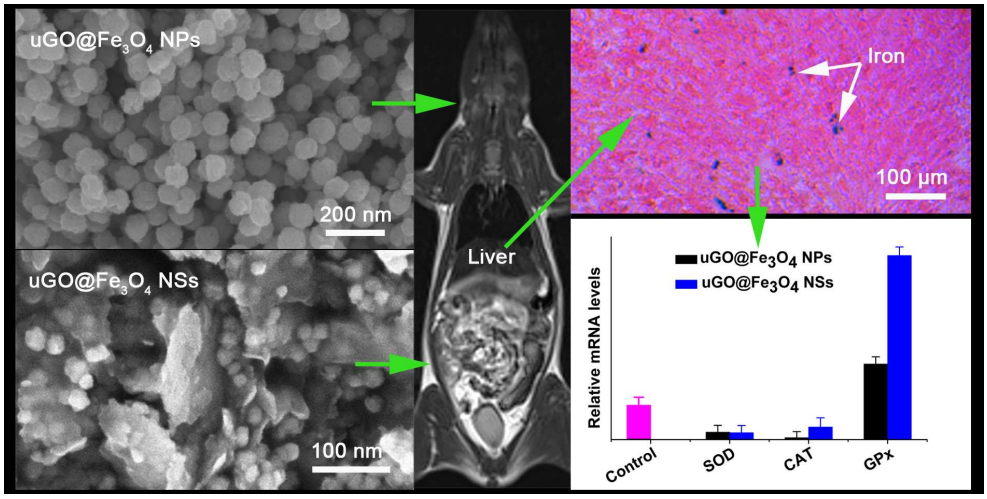

Safety evaluation of graphene oxide-based magnetic nanocomposites.

Safety evaluation of graphene oxide-based magnetic nanocomposites as MRI contrast agent and drug delivery vehicle

Jian-Min Shen[a*], Gang Huang[b], Xing Zhou[b], Jin Zou[a], Yang Yang[a], Yan-Fang Chen[a], Sheng-Kang Men[a]

[a] Department of Biochemistry and Molecular Biology, School of Life Sciences, Lanzhou University, Lanzhou, Gansu 730000, China

[b] The People's Hospital of Gansu Province, Lanzhou, Gansu 730000, China

[*] Corresponding author:Jian-Min Shen. Tel.: +86-15117266908; fax: +86-931-891-5208.
E-mail address: shenjianmin@lzu.edu.cn (Jian-Min Shen)

Abstract:

A variety of graphene oxide-based magnetic nanocomposites have been developed based on the purpose for biomedical applications. However, their safety is still unclear *in vivo*. Here, two nanocomposites of ultrafine graphene oxide-iron oxide nanoparticles and nanosheets (uGO@Fe_3O_4 NPs and NSs) were prepared. The samples were used for evaluating the morphology, dosage, time-dependent effects on various biochemical parameters of clinical significances at various levels: organ, cell, and molecule in a female Wistar mouse model and hepatic cell lines. At the organ level, the explorations of biodistribution, MRI, and histopathology consistently showed that the uGO@Fe_3O_4 NPs and NSs were primarily trapped in the liver and spleen. The heart, liver, spleen, and kidney were damaged based on histopathological observation and the obvious fluctuation of blood biochemical indicators. At the cellular level, the researches of blood compatibility and cytotoxicity demonstrated that the uGO@Fe_3O_4 NSs possessed a higher toxicity than uGO@Fe_3O_4 NPs, and resulted in about 47% (HepG2) and 48% (L02) loss of cell viability at its highest concentration (400 μg Fe/mL). At the molecular level, uGO@Fe_3O_4 NPs and NSs suppressed mRNA expression levels of SOD and upregulated mRNA expression levels of GPx, while the effect on CAT gene expression was mixed, suggesting the significant fluctuation in uGO@Fe_3O_4 nanocomposites-induced oxidative stress in mice. The assessments indicated that the uGO@Fe_3O_4 NPs and NSs have no acute fatal toxicity, but have certain toxicity.

Keywords: Graphene oxide (GO); magnetic nanoparticles (MNPs); toxicity; magnetic resonance imaging (MRI); oxidative stress

1. Introduction

Magnetic nanoparticles (MNPs) with inherent ultrafine size, biodegradability, biocompatibility and superparamagnetic properties are promising material for drug delivery, hyperthermia, targeting, and magnetic resonance imaging (MRI).[1-4] The applicability of MNPs depends to a great degree upon the modification of their functionalization.[5] Coupled with functional moieties including cross-linking agents (e.g. active macromolecules, surfactant, and organic polymer) and ligands (e.g. peptides, antibodies, and small molecules), the resulting hybrids possess more extensive properties than their MNPs precursor, and can be used as drug delivery vehicles and high-performance imaging and diagnostic probes.[6,7] In recent years, graphene oxide (GO), a novel two-dimensional carbon nanostructure, has acquired wide acceptance because of its large specific surface area, monoatomic layer plane, and unique thermal properties.[8-11] Graphene oxide-based magnetic nanoparticles (GO@MNPs) composites, which are usually synthesized by taking GO as substrate material, endow them with excellent qualities.[12] Subsequently, various functionalized GO@MNPs composites were developed based on the purpose for biomedical applications such as contrast agents and drug carriers.[13-15]

Unfortunately, recent evidences have shown GO for use in MRI and drug delivery have health risks.[16] GO was able to induce oxidative stress,[17] plasma membrane damage,[18] changes in gene expression,[19] lung inflammatory response,[20] and strong thrombotoxicity in vitro or in vivo.[21] It is obscure whether GO@MNPs nanocomposites are also so because the hybrids have similar characteristics to GO after all. For example, sheet GO was apt to be intercepted by reticuloendothelial system and caused lung granuloma in mice,[20] and evoked strong aggregatory response in human platelets.[21] Presumably, GO-based magentic nanosheets have the similar potential disadvantages. Therefore, it is necessary to confirm the safety and biocompatibility of GO@MNPs nanocomposites through extensive *in vitro* and *in vivo* studies before being used for MRI and drug delivery. So far, however, to the best of our knowledge, only a few relevant works have been conducted. In some studies, though GO@MNPs nanocomposite was developed for promoting tumor targeting drug delivery and MRI,[12] it is not fully known what toxicity and biodistribution are *in vivo*. Most of the studies solely involved cytotoxicity assay in vitro and concluded that functionalized GO@MNPs nanocomposite is a pretty safe material based on relative cell viability.[13,14] Particularly, GO@MNPs nanocomposite for integrated applications

including drug delivery, photothermal therapy and MRI in vivo was also merely evaluated at cellular level,[15] excepting very few literature.[22] Strictly speaking, however, cultures in vitro cannot completely simulate the complexity of the living system or supply convincing data regarding the response of the physiological system to exogenous agents.[23-25] So far, only Wang et al. carried out the biodistribution of multifunctional magnetic-graphene nanoparticles except for cytotoxicity assay.[26] Additionally, there have been no literatures on the detailed safety evaluation of GO@MNPs nanocomposites in any animal models, which is preferred for the toxicological assessment of a novel material,[23] let alone explored the simultaneous molecular and biochemical responses of antioxidant enzyme and biotransportation in the body. As a consequence, although several groups have presented the use of GO@MNPs nanocomposites for MRI in animals,[12,26] no real clinical MRI applications have been reported so far to our best knowledge, likely because of the lack of biocompatibility evidences of GO@MNPs nanocomposites.

In the present study, we selected two kinds of GO@MNPs nanocomposites with different morphologies as samples, which were synthesized by a solvothermal method for nanoparticles (NPs) or a novel chemical precipitation method developed by us for nanosheets (NSs),[27,28] respectively, used for a systematic toxicity studies. The intravenous administration was carried out to obtain assessment results in vivo.[29] Then, the bio-transportation of GO@MNPs nanocomposites was qualitatively and quantitatively analyzed by MRI observation and iron concentration determination with the inductively coupled plasma optical emission spectroscopy (ICP-OES). Blood compatibility, cytotoxicity, blood biochemical parameters, and histopathology were systematically researched. In addition, we researched oxidative stress-related enzyme gene expression because alterations in these enzyme levels directly reflect the response for organism to exogenous stimulus at the molecular level.[30] Gene expression profiling of superoxide dismutase (SOD), catalase (CAT), and glutathione peroxidase (GPx) from mouse livers of each administration was analyzed by real-time reverse transcriptase polymerase chain reaction (RT-PCR) to further assay nanocomposites-induced hepatotoxicity.

2. Materials and methods

2.1 Materials

Graphite (99.95%) with an average particle diameter of 4 mm, 98% sulfuric acid, sodium nitrate, potassium permanganate, hydrogen peroxide, dimethyformamide (DMF), ferric trichloride

hexahydrate, ethanediol, sodium acetate, polyethyleneglycol-2000 (PEG), iron sulfate heptahydrate, and WST-8 reagent were acquired from Sigma Aldrich (Shanghai, China). All cell lines used in experiment were acquired from the Shanghai cell bank (China). The ultrapure water was used throughout the experiment.

2.2 Synthesis of uGO@Fe_3O_4 nanocomposites

Ultra-fine graphene oxide (uGO) sheets were prepared from expandable graphite powder as described in our previous paper.[28] The spherical uGO@Fe_3O_4 nanoparticles were synthesized by hydrothermal method.[27] In a typical reaction, 2.16 g $FeCl_3 \cdot 6H_2O$, 1.6 g polyethylene glycol (PEG-2000) and 5.76 g NaOAc were thoroughly dissolved in 80 mL ethylene glycol under ultrasonication. Then 320 mg resulting uGO was uniformly dispersed in above mixture via ultrasound for 1 h. After that, the suspension was transferred into a 100 mL Teflon stainless-steel autoclave and reacted at 200 ℃ for 4.5 h. The as-prepared uGO@Fe_3O_4 nanocomposite was washed with deionized water and ethanol and dried at 60 ℃. The product was denoted as uGO@Fe_3O_4 nanoparticles (uGO@Fe_3O_4 NPs). The uGO@Fe_3O_4 nanosheets were prepared by combination of simple one-step chemical deposition and slow oxidation. Specifically, 500 mg of uGO was preprocessed with 30 mL of NaOH solution (0.23 mol/L) under ultrasonication for 40 min, followed by stirring for another two days under nitrogen protection. The suspension was adjusted to pH=8.6 with NaOH solution (6 mol/L) as soon as 2.43 g of $FeSO_4 \cdot 7H_2O$ was added, followed by ultrasonication for 40 min and stirring for 24 h at room temperature. Then, iron ions were oxidated for 2～3 min in the oxygen flow (0.04 m^3/ h) and for 10 min in the air flow (0.1 m^3/ h) while shaking. Afterwards, the suspension was re-adjusted to pH=10.0 and continued to stir for 1 h. The product was separated and completely washed with deionized water by magnetic decantation to remove residual precursors. The product was denoted as uGO@Fe_3O_4 nanosheets (uGO@Fe_3O_4 NSs).

2.3 Characterization and analytical methods

The resulting uGO@Fe_3O_4 NPs/NSs were characterized by X-ray diffraction (XRD) using Cu Kα radiation at X'Pert PRO (PANalytical, Holand). Their external and inner morphology were observed with a scanning electron microscopy (SEM, S-4800, Hitachi, Japan) and transmission electron microscopy (TEM, TecnaiG^2 F30, FEI, USA) with an acceleration voltage of 200 kV, respectively. The composition of the samples was analyzed by a Fourier transform infrared (FT-IR)

spectrometer (NEXUS 670 FT-IR，Nicolet，USA). The FT-IR spectrum was collected between the wave number of 400 and 4000 cm^{-1}. The size and zeta potential of the uGO@Fe_3O_4 NPs/NSs suspended in HSA (0.6 mM)-containing PBS media at pH 7.4 were determined using a Malvern dynamic light scattering (DLS) (Zetasizer Nano 3600, U.K.) in triplicate.

2.4 In vitro magnetic property evaluation (VSM and MRI)

The magnetization saturation properties of uGO@Fe_3O_4 NPs/NSs were measured on a Lake Shore vibrating sample magnetometer (VSM). For MRI studies, different concentrations (0, 1.25, 2.5, 5.0, 10.0, 20.0 μg Fe/mL) of uGO@Fe_3O_4 NPs/NSs were suspended in a total volume of 1.5 mL agar phantoms (1.5%, w/v) without air bubbles in a 24-well plate. MR images of agar phantoms were acquired using a Siemens Skyra machine operating at 3.0 T, horizontal bore MRI scanner equipped with a dedicated knee joint coil (15 channels). T2 relaxation times were determined using following sequence parameters: repetition time (TR) 2400 ms, echo time (TE) 67 ms, matrix size 256×320, field of view (FOV) 161×161 mm, slice thickness 3 mm. MR image analyses were conducted using the Siemens multi modality work place (MMWP) with software Vision VE40.

2.5 Haemocompatibility assessment in vitro

2.5.1 Hemolysis assay

For hemolysis study, 2 mL of healthy human blood (Red Cross Blood Center, Gansu, China) was centrifugated at 1500 rpm for 10 min to collect human red blood cells (HRBCs). HRBCs were redispersed in 10-fold volume of sterile PBS media. 100 microliter of HRBCs suspension was treated with (a)1.9 mL of uGO@Fe_3O_4 NPs/NSs in PBS at concentrations of 12.5, 25, 50, 100, 200, and 400 μg Fe/mL as samples; (b) 1.9 mL of PBS as a negative control; (c) 1.9 mL of deionized water as a positive control. The cells were incubated at a standstill for 3 h at 37 ℃ after shaken gently. The mixtures were centrifuged at 1500 rpm for 10 min, and the haemolysis degree was determined by recording absorbance values of the supernatant at 541 nm. The hemolysis percentages of the samples were calculated according to the equation below:[31]

$$\left(\text{Sample O.D.}_{541}-\text{Negative control O.D.}_{541}\right)/\left(\text{Positive control O.D.}_{541}-\text{Negative control O.D.}_{541}\right)\times 100\%$$

2.5.2 Coagulation assay

100 microliter of fresh human plasma was treated with (a) 900 μL of uGO@Fe_3O_4 NPs/NSs in

PBS at concentrations of 12.5, 25, 50, 100, 200, and 400 μg Fe/mL as samples; (b) 900 μL of PBS as a control. The mixtures were incubated at 37 ℃ for 5 min and centrifuged at 2500 rpm for 10 min. The supernatants were used to analyze prothrombin time (PT) and activated-partial-thromboplastin time (APTT) on a fully automatic blood-coagulation analyzer (ACL TOP 9000, USA) by using the SynthAsil kit (Instrumentation Laboratory Company, Orangeburg, USA).

2.6 Cytotoxicity and apoptosis assay in vitro

In vitro cytotoxicity was assessed using a WST-8 test and FITC-labeled Annexin-V and propidium iodide (PI) staining. Human hepatocytes cancer HepG2 cells and normal hepatocytes L02 cells were used for this experiment. Cells were seeded in 96-well plates at a density of 1×10^4 cells/well in RPMI-1640 medium and incubated with uGO@Fe_3O_4 NPs/NSs with different concentration (12.5～400 μg Fe/mL, in PBS) for 24 h. Equivalent amount of PBS without nanocomposites was used as control. Then, cells were washed twice with PBS and the WST-8 reagent was added to each well. After incubation for 30 min, the absorbance was determined on a microplate spectrophotometer at 460 nm. The blank absorbance (medium without cells) was subtracted from each value. All the experiments were conducted in triplicate. For the detection of nanocomposite-induced apoptosis, the cells treated with uGO@Fe_3O_4 NPs/NSs were stained with Annexin-V/PI and analyzed by flow cytometer (BD LSRFortessa, USA).

2.7 Animals and treatment regime

Female Wistar mice (BW 150–200 g) were supplied by the Experimental Animal Center of Lanzhou University (Lanzhou, China). The animals were housed (2/cage) at 22 ± 1℃ under a 12-h light:12-h dark cycle and 50-60% relative humidity with free access to standard pellet diet and tap water. All experiments were conducted in accordance with the protocols approved by the Ethics Committee of Animal Experiments of Lanzhou University. Animals were randomly divided into seven groups: a control group and six sample groups (low, medium, and high dose groups per composite). The sample group mice were injected with suspension containing uGO@Fe_3O_4 NPs/NSs in sterile PBS irradiated by ^{60}Co by a lateral tail vein (0.5 mL per mouse, 5, 7.5, 10 mg Fe/kg body weight), respectively. The control group mice were given 0.5 mL of sterile PBS. Five mice from each group were weighed and sacrificed at regular time points (1 h, 24 h, 7 days and 14 days). Firstly, blood was collected using a standard vein blood collection technique for Fe

concentrations and biochemistry assay. Then, heart, liver, spleen, lung and kidney were immediately excised. A piece of tissue (0.5×0.5×0.3 cm) was quickly removed and fixed with 4% paraform for 48 h for further histopathological examinations. After dehydrated progressively, the fixed sections were embedded in paraffin, sectioned, and stained with H&E and Prussian Blue standard protocol (Table S1). All the residual tissues were stored at -80 ℃ for analysis of bio-transportation of ferrofluid *in vivo* and gene expression.

2.8 Quantitative analysis of Fe concentrations by ICP-OES

The iron concentrations in blood and organs at different doses (5, 7.5, 10 mg Fe/kg) and times (1 h, 24 h, 7 days and 14 days) were analyzed by ICP-OES (IRIS ER/S, TJA, USA). Samples were prepared by complete digestion of blood (3 mL) and organs (300～500 mg) in 2 mL of mixed solution of nitric acid and perchloric acid with a volume ratio of 10:1 at 90 ℃ for 4 h. The digested solution was cooled and diluted to 5 mL of constant volume with deionized water for Fe concentration measurement. Fe concentration in specific tissue of different administrations was expressed as mass per milliliter of blood (Fe μg/mL) or per gram of tissue (Fe μg//g).

2.9 Blood biochemical assays

For blood biochemical assays, 1.0 mL of the blood sample was centrifuged at 2000 rpm for 10 min. The serum samples were used for measuring the following parameters using a biochemical autoanalyzer (Accute 400, Toshiba, Japan): total bilirubin levels (TBIL [μmol/L]), albumin (ALB [g/L]), alanine aminotransferase (ALT [U/L]), aspartate aminotransferase (AST [U/L]), alkaline phosphatase (ALP [U/L]), blood urea nitrogen (BUN [mmol/L]), creatinine (CREA [μmol/L]), and lactate dehydrogenase (LDH [U/L]).

2.10 In vivo magnetic resonance imaging (MRI)

Three mice from low dose group treated with uGO@Fe_3O_4 NPs or NSs were weighed and anesthetized with 20% urethane. MR images were acquired using a 3.0 T system (Siemens Skyra), horizontal bore MRI scanner equipped with a dedicated knee joint coil (15 channels). The turbo spin echo (TSE) technique was applied with acquisitions in the T2-weighted sequence in the coronal plane. T2-weighted image parameters were as follows: TR 3000 ms, TE 67 ms, NEX 4, matrix size 256 × 256, FOV 190 × 190 mm, slice thickness 2 mm.

2.11 RNA extraction and gene expression

Total hepatic RNA was extracted and purified from liver tissues treated with uGO@Fe_3O_4 NPs

or uGO@Fe_3O_4 NSs at different doses (5, 7.5, 10 mg Fe/kg) for 14 days and blank control liver using a Takara™ reagent (Shiga, Japan), according to the manufacturer's instructions. The quality of total RNA was assessed by AGE (agarose gel electrophoresis) and determining the ratio of A260/A280 on a UV spectrophotometer (Bio Teke ND5000, China). The purified RNA was stored at −80 ℃ for further use. cDNA was prepared and detected on a Lang gel imaging system (LG2020D, Hangzhou, China) based on obtained RNA for quantitative RT-PCR assay as described in the instructions of PrimeScript™ RT reagent Kit (Japan). The PCR fluorescent quantitation was carried out in a 15.3 μL system with a SYBR Premix Ex Taq™ Kit (Takara, Japan), 2 μL of specific upstream primer and 2 μL of specific downstream primer (Table 1), synthesized by SBS Genetech Co.,Ltd, Shanghai, China, and 1 μL of cDNA using the following procedure: initial denaturation at 95 °C for 120 s followed by 45 cycles of amplification (95 °C for 15 s and 60 °C for 40 s). The same operation was performed in triplicate. The target genes evaluated involved SOD, CAT, and GPx. GAPDH was selected as internal standard primer. Fluorescent quantitative PCR was performed on a real-time QPCR system (Stratagene MX3005P, USA).

Table 1

Sequences of qPCR primers used in the experiment.

Gene	Upstream primer sequences (5′–3′)	Downstream primer sequences (5′–3′)
SOD	CCACTGCAGGACCTCATTTT	CACCTTTGCCCAAGTCATCT
CAT	CGACCGAGGGATTCCAGATG	ATCCGGGTCTTCCTGTGCAA
GPx	TGCCCTACCCTTATGACGAC	TCGATGTTGATGGTCTGGAA
GAPDH	ATGGAGAAGGCTGGGGCTCACCT	AGCCCTTCCACGATGCCAAAGTTGT

2.12 Statistical analysis

Data represent mean±standard error of the mean (S.E.M.). Statistical analyses between the samples and the controls were conducted using ANOVA. All the graphs were plotted using Origin 8.5 software.

3. Results

3.1 Characterization of uGO@Fe_3O_4 nanocomposites

The morphologies of uGO@Fe_3O_4 NPs/NSs are shown in the TEM and SEM images (Figure 1).

Figure 1A and C consistently demonstrate that uGO@Fe_3O_4 NPs tend to sphere and a narrow range of distribution (approximately 80±10 nm) based on statistical data of 100 particles. The average diameter of NPs was consistent with that measured from the DLS (Figure 2A). uGO and Fe_3O_4 MNPs in composites are uniformly bound together and cannot be distinguished. In the case of uGO@Fe_3O_4 NSs, it can be clearly observed that Fe_3O_4 MNPs of less than 20 nm in size are uniformly decorated onto uGO sheets (Figure 1B and D), and the average size of nanosheets was also about 80±10 nm based on 100 particles by TEM and SEM images. In order to assess stability of uGO - iron oxide composites, uGO@Fe_3O_4 NPs or NSs were soaked in HSA (0.6 mM)-containing PBS media at pH 7.4 for 14 days, and then were washed with deionized water. The iron loading efficiencies were almost the same before and after immersion, and accounted for 49.6 wt % for uGO@Fe_3O_4 NPs and 48.5 wt % for uGO@Fe_3O_4 NSs by ICP-OES measurement.

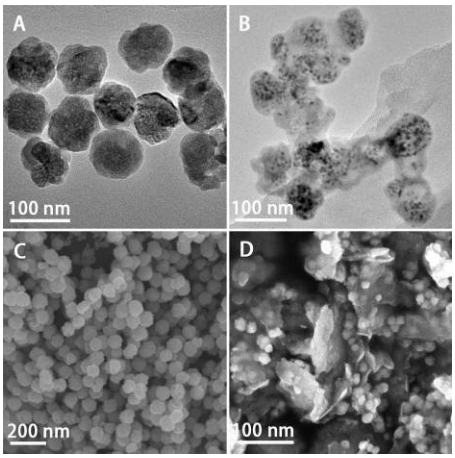

Figure 1. (A) TEM and (C) SEM images of uGO@Fe_3O_4 NPs. (B) TEM and (D) SEM images of uGO@Fe_3O_4 NSs.

In order to determine the zeta-potentials of the uGO@Fe_3O_4 NPs and NSs in simulative physiological environment, a HSA (0.6 mM)-containing PBS medium was used.[28] In this medium, uGO@Fe_3O_4 NPs possessed higher negative ζ potential of about −33.8 than NSs (−28 mV) at room temperature (Figure 2B), reflecting spherical NPs synthesized by hydrothermal method exist more carboxyl group exposure than NSs prepared by chemical deposition method.

Based on the profiles of the XRD spectra, the characteristic peaks of uGO@Fe_3O_4 NPs and NSs at (111), (220), (311), (400), (511), (422) and (440) (Figure 2C) demonstrated the presence of magnetic nanoparticles. In addition, no peaks corresponding to other crystallographic structure were observed, testifying the purity of two kinds of hybrids. Similar intensity peaks can be seen in uGO@Fe_3O_4 NPs and NSs, indicating that there were almost the same magnetic nanoparticles

content in the two kinds of nanocomposites.

The FTIR spectra shown in Figure 2D were used to determine the composition of uGO@Fe_3O_4 NPs and NSs. Whether in uGO@Fe_3O_4 NPs or in NSs, the characteristic peaks corresponding to the stretching vibration of hydroxy group at 3400 cm^{-1}, carboxyl group at 1735 cm^{-1}, and the Fe−O bond at 590 cm^{-1} clearly indicated the successful preparation of uGO@Fe_3O_4 hybrids.

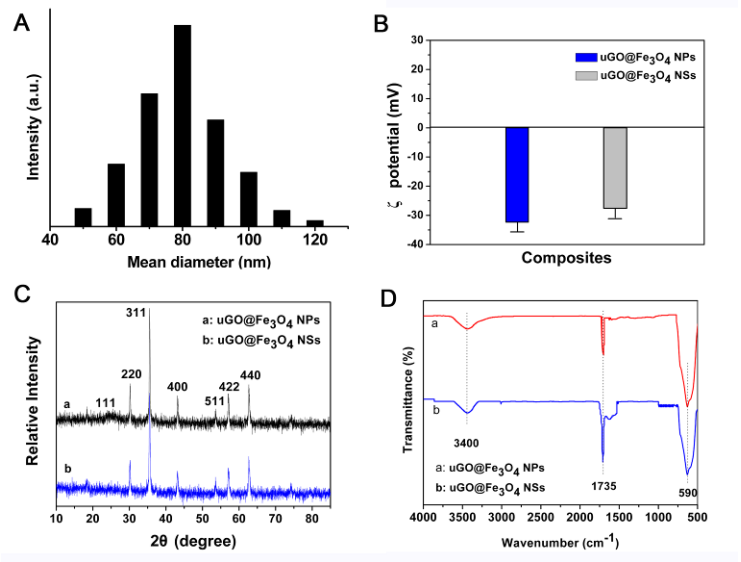

Figure 2. (A) The size distribution of uGO@Fe_3O_4 NPs. (B) ξ-potentials, (C) XRD, and (D) FTIR spectra of uGO@Fe_3O_4 NPs and NSs. The size distributions and ξ-potentials of nanocomposites were measured in HSA (0.6 mM)-containing PBS media at pH 7.4. The size distribution of NSs was not presented because DLS cannot describe non-spherical particles well.

3.2 Magnetization property in vitro

The magnetization properties of uGO@Fe_3O_4 NPs and NSs were measured at room temperature, as shown in Figure 3A. Although the uGO@Fe_3O_4 NPs and NSs were synthesized with the different methods and had different morphologies, their saturation magnetization intensity was very close, reaching 49 emu/g for NPs and 53 emu/g for NSs, respectively. This can completely make an adequate magnetic responsiveness in the applications for MR imaging and magnetic induction based on our previous study.[28]

To further demonstrate the effect of bound Fe_3O_4 MNPs on T_2 relaxation, a 24-well plate containing MNPs, uGO@Fe_3O_4 NPs, uGO@Fe_3O_4 NSs, and uGO suspended in 1.5 mL of 1.5% agar phantoms with the different iron concentrations were imaged using a 3T MRI instrument (Figure 3B). Fe_3O_4 MNP was taken as a control to provide a reference for uGO@Fe_3O_4 NPs and NSs. Fe_3O_4 MNPs can lead to decrease in regional signal intensity due to reducing of T_2 relaxation time.[7] It was obvious that signal gradually decreased as the concentration of Fe_3O_4 MNPs in the

uGO@Fe_3O_4 hybrids enhanced from 1.25 μg Fe/mL to 20 μg Fe/mL. Relative to the sole MNPs- or uGO-containing gel, uGO@Fe_3O_4 NPs and NSs possessed higher signal than pure MNPs and lower than uGO. The obtained images were used to plot a $1/T_2$ map (Figure 3C). The transverse relaxation rate ($1/T_2$), as a function of the Fe concentration in each formulation, increased linearly with the Fe concentration in all the samples (Figure 3C). The $1/T_2$ displayed to increase in the following order for the tested samples: uGO＜uGO@Fe_3O_4 NPs＜uGO@Fe_3O_4 NSs＜MNP. As a consequence, the uGO@Fe_3O_4 NPs and uGO@Fe_3O_4 NSs can potentially perfect observation by contrast enhancement using T_2-weighted imaging process.

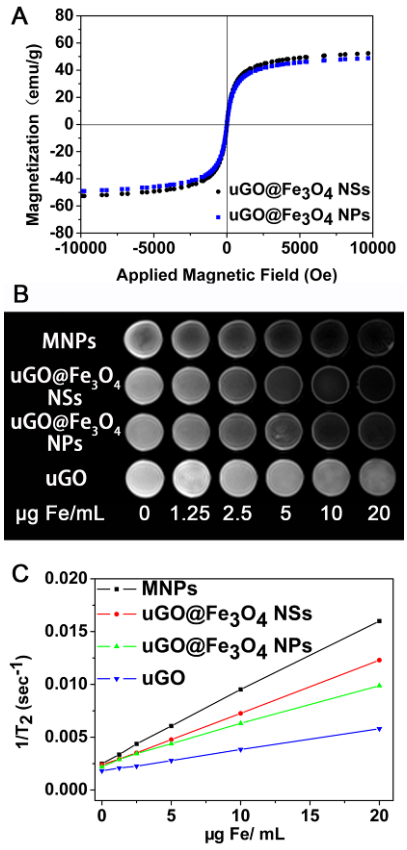

Figure 3. (A) Magnetization curve and (B,C) magnetic resonance image (MRI) characteristics of uGO@Fe_3O_4 NPs and NSs formulations. (B) The plate was loaded with the different concentrations of uGO@Fe_3O_4 NPs or NSs suspended in 1.5 mL of 1.5% agar phantoms at 25 ℃and imaged with a 3.0 T Siemens Skyra MRI instrument, respectively. (C) T_2 relaxation rates ($1/T_2$) plotted as a function of the Fe concentration for uGO@Fe_3O_4 NPs and NSs formulations.

3.3 Haemocompatibility assays in vitro

The research indicated that no significant hemolysis effects were found for uGO@Fe_3O_4 NPs and NSs formulations in the range of 12.5～400 μg Fe/mL of concentration (Figure 4A and B). Particularly, uGO@Fe_3O_4 NPs did not display any hemolytic activity even at 400 μg Fe/mL of

high concentration, as low as 1.65% hemolysis percentage was monitored, and still fell within the negligible scope (＜5%).[32] By contrast, a 4.43% hemolysis percentage was detected for uGO@Fe_3O_4 NSs at this concentration. Figure 4C demonstrated that PT values of plasma exposed to uGO@Fe_3O_4 NSs or uGO@Fe_3O_4 NPs in the range of 12.5～100 μg Fe/mL of concentration were within their normal ranges of 11～13 s,[33] respectively. However, as the concentration of uGO@Fe_3O_4 NSs or uGO@Fe_3O_4 NPs increased, the PT values reduced to below normal ranges. Figure 4D showed that APTT values of plasma exposed to two kinds of nanocomposites in all test concentration range were within their normal ranges of 25.4～38.4 s,[34] respectively.

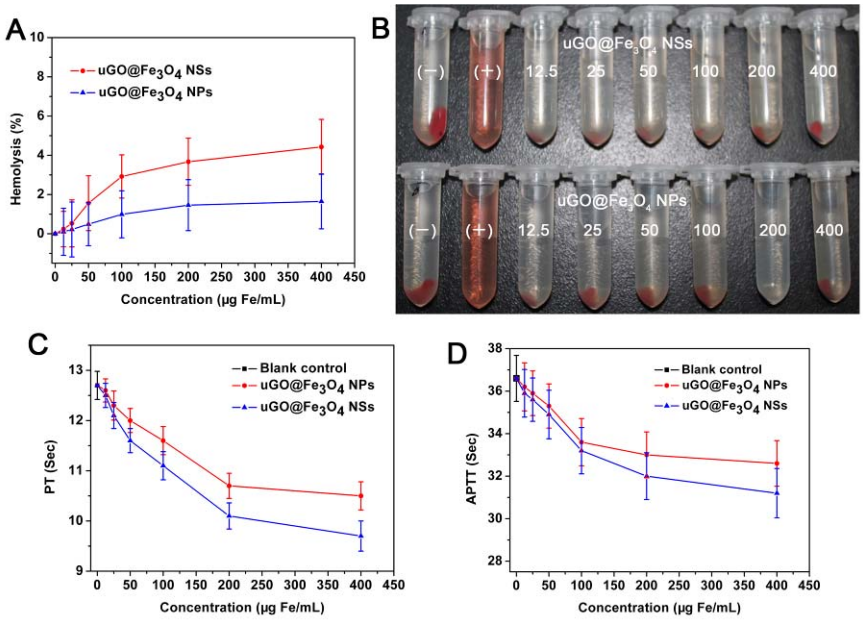

Figure 4. Blood compatibility studies *in vitro*. (A) Hemolysis percentages of uGO@Fe_3O_4 NPs and NSs formulations in PBS at the concentrations of 12.5, 25, 50, 100, 200, and 400 μg Fe/mL. (B) Representative photograph of the hemolysis assay to detect the presence of hemoglobin in the supernatant of formulations in PBS at above concentrations. + and − symbols represent positive control and negative control, respectively. (C) and (D) Coagulation properties of uGO@Fe_3O_4 NPs and NSs formulations at above concentrations after incubation with fresh plasma for 5 min.

3.4 Cytotoxicity and apoptosis assay in vitro

Human hepatocytes cancer HepG2 cells and normal hepatocytes L02 cells are classical *in vitro* models applied to hepatotoxicity research. As shown in Figure 5A and 5B, uGO@Fe_3O_4 NPs showed higher cell viabilities for HepG2 cells and L02 cells than uGO@Fe_3O_4 NSs at all tested concentrations according to the WST-8 assay. Even though at 400 μg Fe/mL of high concentration, uGO@Fe_3O_4 NPs still revealed high cell viabilities for HepG2 cells (70%) and L02 cells (65%). To further perform a quantitative comparison regarding apoptosis induced by uGO@Fe_3O_4 NPs or uGO@Fe_3O_4 NSs, above HepG2 and L02 cells treated with nanocomposites were co-stained with

annexin V/PI to detect on a laser scanning confocal microscope (LSCM) and analyze by flow cytometry. It is clear that after treated with uGO@Fe_3O_4 NPs or uGO@Fe_3O_4 NSs, some HepG2 and L02 cells display significant green fluorescence cytoplasm and red fluorescence nucleus (herein only present HepG2 cells, Figure 5C) compared with control cells untreated (inset in Figure 5C).

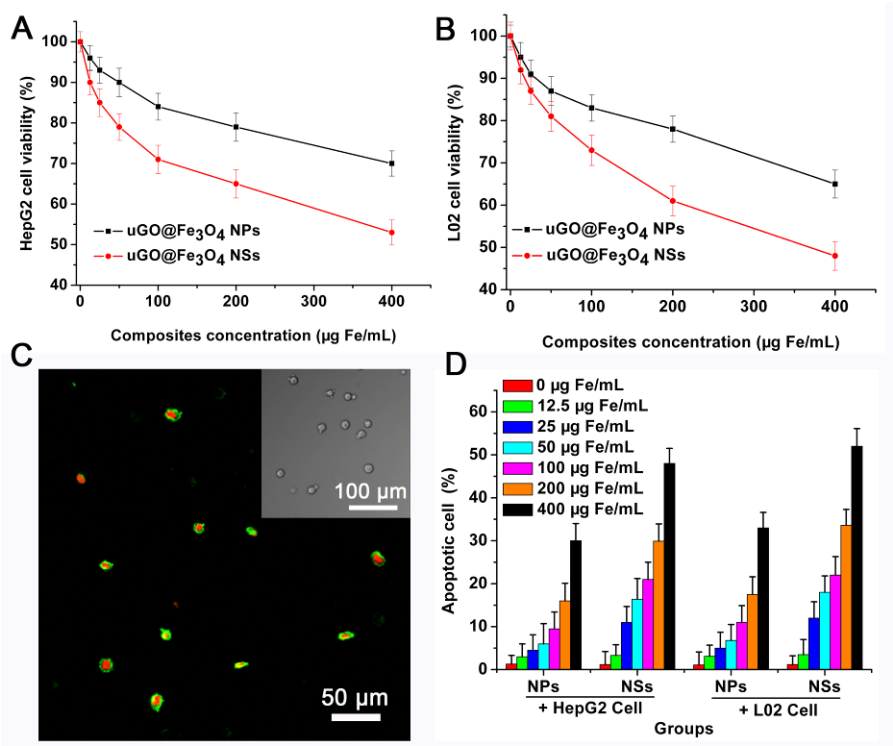

Figure 5. (A) and (B) *In vitro* cell viabilities of the uGO@Fe_3O_4 NPs or uGO@Fe_3O_4 NSs with different concentrations against HepG2 cells and L02 cells were determined using WST-8 assay. (C) Representative HepG2 cells (1×10^5 cells/mL in PBS) co-stained with annexin V/PI after treated with uGO@Fe_3O_4 NSs for 24 h. The inset in right top in (C) is control image (untreated cells) to compare them to. (D) Quantification of apoptotic cells after treated with uGO@Fe_3O_4 NPs or uGO@Fe_3O_4 NSs using annexin V/PI co-staining and analysis by flow cytometry. Mean values ± SD (n = 5) are plotted.

3.5 Blood biochemical assays

In this section, living mice were intravenously administrated with uGO@Fe_3O_4 NPs or NSs according to the three doses (5, 7.5, and 10 mg Fe/kg). The blood biochemical indicators were shown in Figure 6. The results indicated that TBIL, ALT, AST, ALP, BUN, and LDH have elevated, to different extents, compared with the control (Figure 6). Particularly, *in vivo* a high dosage-exposure of uGO@Fe_3O_4 NPs and NSs induced more obvious increase in these indicator levels than low dosage. By contrast, ALB level in the serum declined compared to the control group ($p < 0.05$) (Figure 6B), and CREA data there was not significant difference between the

sample groups and the control (Figure 6G). The results of 14 days after injecting uGO@Fe_3O_4 NPs or NSs were not presented because of a roughly parallel to the data on the seventh day.

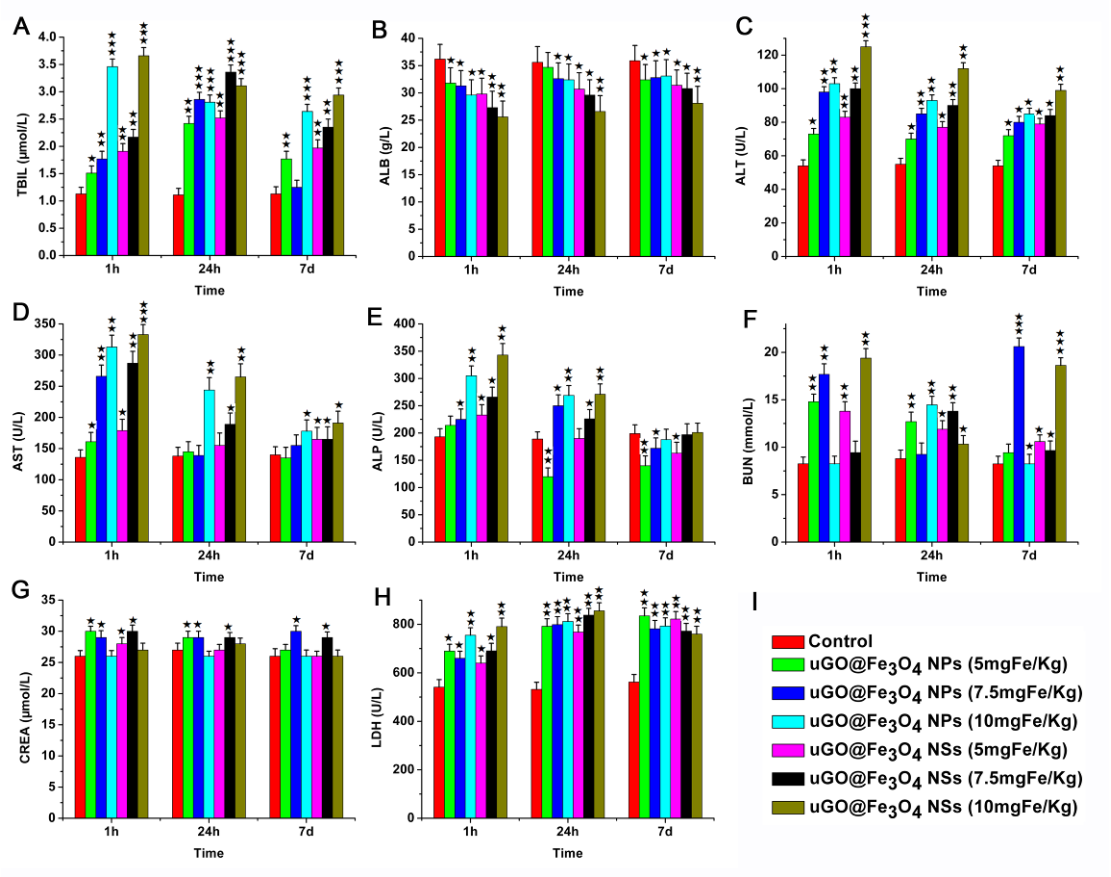

Figure 6. Blood biochemical parameters after injecting uGO@Fe_3O_4 NPs and NSs formulations with different dosages at 1 h, 24 h, and 7 days. Related blood biochemistry indicators: total bilirubin levels (TBIL), albumin (ALB), alanine aminotransferase (ALT), aspartate aminotransferase (AST), alkaline phosphatase (ALP), urea nitrogen (BUN), creatinine (CREA), and lactate dehydrogenase (LDH). All data are presented as mean ± S.E.M. (n=5). $^{\star}p<0.05$, $^{\star\star}p<0.01$, and $^{\star\star\star}p<0.001$ versus control according to ANOVA.

3.6 Biodistribution of GO@MNPs nanocomposites

The ICP-OES measurements were used to assay iron concentration to determine the *in vivo* biodistribution of the uGO@Fe_3O_4 NPs and NSs in mice. The major organs, including blood, heart, liver, spleen, lung, and kidney were collected for iron content determination at 1 h, 24 h, 7d and 14 d after intravenous administration. Figure 7 shows that the iron concentrations in six tissues at different dosages and times changed. The Fe concentrations of control mice only given sterile PBS were expressed as line starting at t = 0 h. In the bloodstream, two kinds of nanocomposites shared a similar circulation pattern, where Fe concentrations were maximized at 1 h post-injection and were basically positively related with the dosage (Figure 7A). At 14 days after intravenous

injection Fe concentrations mostly backed to the value preinjection, showing Fe element was slowly removed from blood plasma. In low doses of uGO@Fe_3O_4 NPs treatment mice (5 and 7.5 mg Fe/kg), the Fe concentration in the heart reached maximum at 1 h after injection. But in mice treated with high doses of uGO@Fe_3O_4 NPs (10 mg Fe/kg) and three doses of uGO@Fe_3O_4 NSs, the peak values of iron in the heart presented at 24 h after injection (Figure 7B). On 14 days after the injection, Fe concentration in the heart treated with uGO@Fe_3O_4 NPs reduced to the level preinjection, while the heart treated with uGO@Fe_3O_4 NSs still remained a small quantity of iron element. The total concentration of Fe accumulated in the liver treated with NPs or NSs always increased with time, while the total concentration of Fe in the spleen originally dramatically increased and subsequently kept constant or slightly decreased (Figure 7C and D). In the lung (Figure 7E), Fe concentrations in uGO@Fe_3O_4 NPs groups had a similar change trend to NSs groups, in other words, 24 h after injection, the iron concentrations were reached the peak, and then gradually declined over the next 13 days. In the kidney, the Fe concentration in the mice treated with uGO@Fe_3O_4 NPs first rapidly increased and then decreased (Figure 7F). By contrast, in the case of uGO@Fe_3O_4 NSs, the Fe concentrations slowly increased within 7 days after the injection and then dramatically increased.

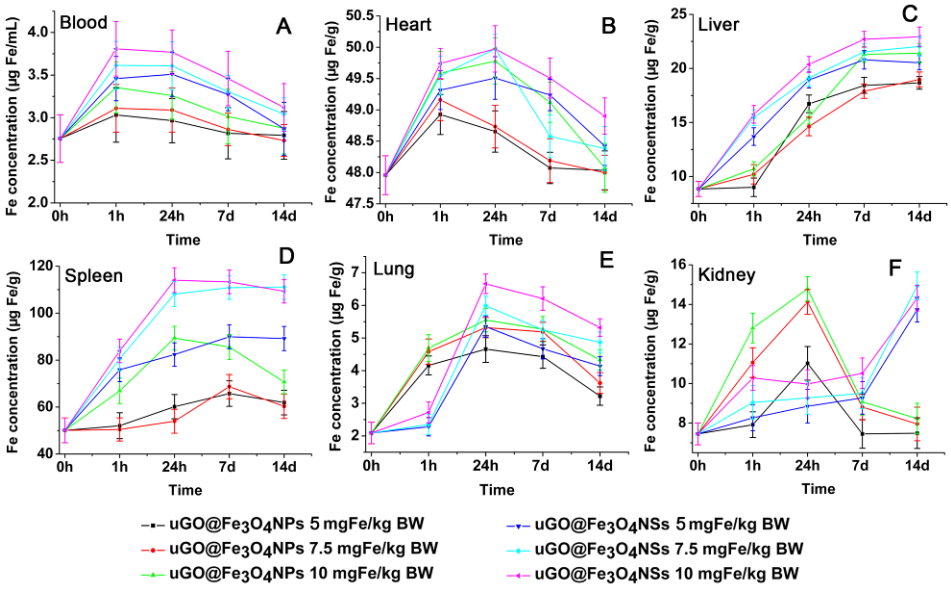

Figure 7. Biodistribution of Fe in tissues from the mice treated with uGO@Fe_3O_4 NPs or NSs with 5, 7.5, and 10 mg Fe/kg doses at different time point. Data point at 0 h represents the quantity of Fe in the organs of control group. Vertical axis means Fe mass per milliliter of blood (μg/mL) or per gram of tissue (μg/g). The data are expressed as mean±S.D. (n = 5).

3.7 MR Imaging in vivo

In order to further explore the dynamic changes of the nanocomposites in the liver, spleen, and kidney, *in vivo* MR imaging was performed using an optimized sequence at echo time 67 ms and repetition time 3000 ms on the 3.0 T MRI instrument. Figure 8A shows representative T_2-weighted MRI images of the same mouse coronal plane before and after intravenous administration of uGO@Fe_3O_4 NSs or uGO@Fe_3O_4 NPs. The liver and spleen apparently darkened, and other organs just a little darkened following the intravenous administration of uGO@Fe_3O_4 NSs or NPs compared with the control Figure 8A(c), reflecting enhancement of the contrast due to the uptake of uGO@Fe_3O_4 nanocomposites in liver and spleen. Especially, the regional signal intensity of mouse liver treated with uGO@Fe_3O_4 NSs was lower than those with uGO@Fe_3O_4 NPs. As shown in Figure 8B and C, the relative signal intensities of liver were 40% and 50% 1 hour after injection of uGO@Fe_3O_4 NSs or NPs, respectively. With time, however, the signal intensity of liver treated with uGO@Fe_3O_4 NSs or NPs was roughly stable. In spleen, the relative signal intensity persistently decreased except at 3h after uGO@Fe_3O_4 NSs were injected, while the signal appeared fluctuation after injection of uGO@Fe_3O_4 NPs. In kidney treated with uGO@Fe_3O_4 NSs, furthermore, the signal variation was small within 7 days, but the signal significantly decreased 7 days later, showing that nanosheets began to be eliminated after continuous accumulation in the kidney for 7 days. In kidney treated with uGO@Fe_3O_4 NPs, by contrast, the signal slowly fell during 6 hours to 24 hours after administration, and then gradually rose. To further verify the uptake of uGO@Fe_3O_4 NSs and NPs in liver and spleen as described by MRI detection, Prussian blue staining of slides from two organs was achieved. The results were presented in supplementary material Figure S2. The histopathological observation indicated that liver of exposure to uGO@Fe_3O_4 NSs generated a time-dependent liver inflammatory response characterized by granulomas (G), swollen vacuolated bundles (S), and interstitial edema (E) (Figure S2 (A) and (B)). Over time, the toxicity reaction of the liver of mice becomes more and more severe. Some inflammation cells were infiltrated in liver interstitium. The hepatic architecture of mice showed some deformation.

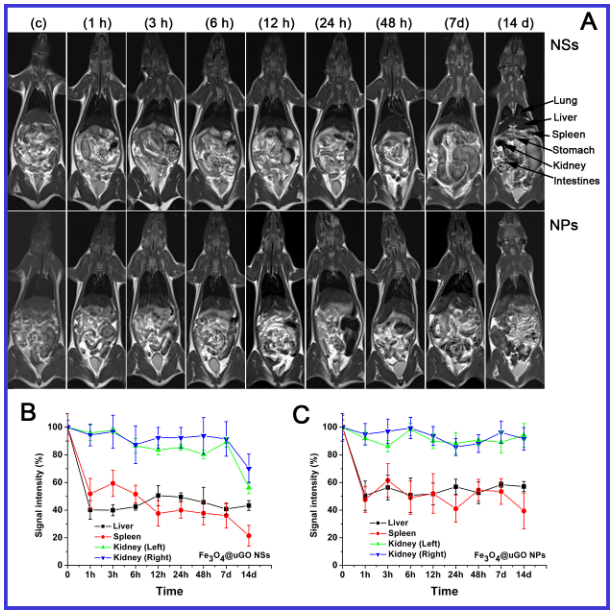

Figure 8. (A) *In vivo* T_2-weighted MR images of the same living mouse obtained by a magnetic resonance instrument before (control, c) and after (1h, 3h, 6h, 12h, 24h, 48h, 7d, and 14d) intravenous administration of sterile saline solution containing uGO@Fe_3O_4 NSs or NPs (5 mg Fe/kg). (B) and (C) Time dependence of the relative signal intensity in liver, spleen, and kidneys after the administration of uGO@Fe_3O_4 NSs or NPs.

3.8 Gene expression

Herein, RT-PCR of hepatic mRNA under different treatment modes has been performed to further analyze uGO@Fe_3O_4 NPs/NSs-induced oxidative stress behavior. The identification data of PCR products were presented in supplementary material Table S3, Figure S4, and Figure S5. Figure 9 illustrates the effect of uGO@Fe_3O_4 NPs or NSs with various doses on mRNA expression of SOD, CAT, and GPx 14 days after injecting. As depicted in Figure 9, uGO@Fe_3O_4 NPs and NSs caused significant decrease in the expressions of SOD mRNA gene (Figure 9A) and substantial increase in the expressions of GPx mRNA gene (Figure 9C) compared with the control ($p<0.01$). Especially, uGO@Fe_3O_4 NSs at the dosages of 5, 7.5, and 10 mg Fe/kg caused 4.9, 5.2, 8.3-fold decrease in SOD gene expressions and 5.4, 12.1, 23.1-fold increase in GPx gene expressions compared to the control, respectively. By contrast, the alterations in CAT mRNA gene expression showed complicated situations, where uGO@Fe_3O_4 NPs at the dosages of 5 and 7.5 mg Fe/kg caused about 17.8 and 2.2-fold decrease in hepatic CAT gene expression, and uGO@Fe_3O_4 NSs at the same dosage caused about 2.7 and 3.8-fold decrease compared to the control ($p<0.01$), respectively (Figure 9B). However, there were about 1.3 and 2.0-fold increase in CAT gene expression caused by uGO@Fe_3O_4 NPs and NSs at the doses of 10 mg Fe/kg relative

to control, respectively.

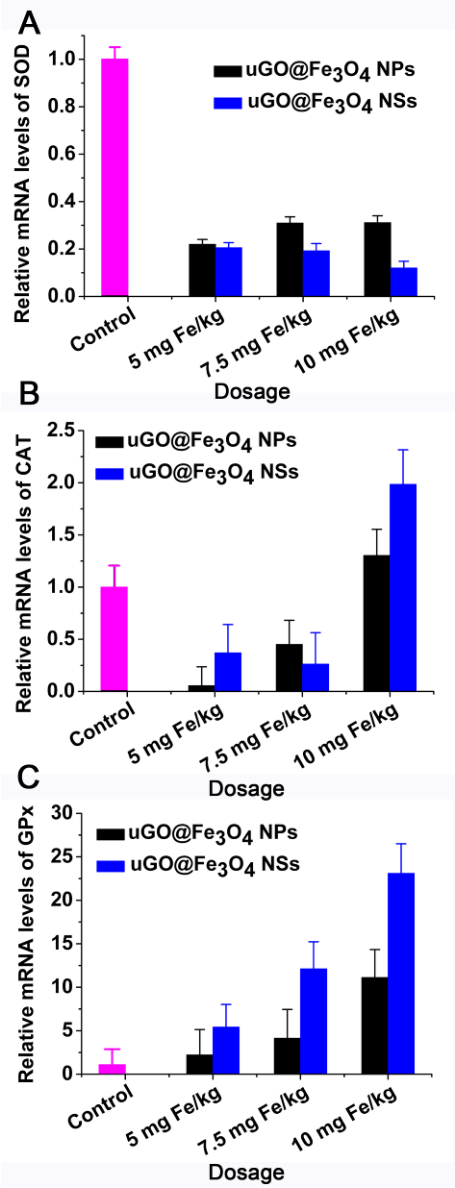

Figure 9. Relative mRNA levels of SOD (A), CAT (B), and GPx (C) from the mouse livers under various doses 14 days after injecting. The data are expressed as mean±S.D. (n=3). $^{\star}p<0.05$, $^{\star\star}p<0.01$, and $^{\star\star\star}p<0.001$ versus control according to ANOVA.

4. Discussion

4.1 Calculation of effective dose

It is essential to determine effective dose of GO-based magnetic nanocomposites to meet MRI contrast demand *in vivo*. Here, in order to relate these two exposures *in vivo* and *in vitro*, the dosages of uGO@Fe_3O_4 NPs or NSs were converted to iron concentration according to the iron loading efficiencies (49.6 wt % for uGO@Fe_3O_4 NPs and 48.5 wt % for uGO@Fe_3O_4 NSs). Female Wistar mice were treated with the dosage magnitude of 5～10 mg Fe/kg BW by

intravenous injection based on the references for similar works for MRI contrast purpose and our practical exploration.[6,35] According to our test, the whole blood of a Wistar mouse (BW 150–200 g) has about 8～10 milliliters by a standard vein blood collection technique. From this calculation, the Fe concentration in blood is about ＜100 μg Fe/mL at that moment of injecting. As a reference, the dosage range of 12.5～400 μg Fe/mL was used for haemocompatibility and cytotoxicity assay *in vitro*.

4.2 Haemocompatibility assays in vitro

Good haemocompatibility is extremely important when nanomaterials enter circulation after vein injection. Hemolysis and coagulation parameters are the most frequently conducted assays for detecting hemoglobin release and thrombosis.[34,36] The research showed that although hemolysis effects fell in the range of security, a higher hemolysis percentage was detected for uGO@Fe_3O_4 NSs compared with uGO@Fe_3O_4 NPs (Figure 4A,B). It was reported that the particle size and exfoliation extent of GO can influence hemolytic activity.[36] In the present case, the sizes of uGO@Fe_3O_4 NPs and uGO@Fe_3O_4 NSs are almost the same (approximately 80 nm) (Figure 1), and their GO moieties were derived from the same batch of uGO with the same exfoliation extent. The hemolytic difference of two nanomaterials is highly dependent on their morphologies.[16] Chen et al. declared that nanocomposite with sharp edges possessed higher toxicity.[37] So, uGO@Fe_3O_4 NSs induced higher hemolysis than uGO@Fe_3O_4 NPs because the former easily penetrate into cells to cause release of free hemoglobin in the medium.[18]

Coagulation evaluation, such as prothrombin time (PT) and activated partial thromboplastin time (APTT) test, is essential for monitoring thrombosis effect caused by exogenetic materials.[38] The study displayed that uGO@Fe_3O_4 NSs or uGO@Fe_3O_4 NPs at low concentration (＜100 μg Fe/mL) did not induce extrinsic coagulation (PT), but the PT values of the plasma mixed with high concentrations (＞200 μg Fe/mL) of nanocomposites obviously declined, even below normal value (11 s) (Figure 4C), reflecting dosage-dependent effects on extrinsic coagulation. By contrast, APTT values did not break through the normal range at all tested concentrations (Figure 4D), showing that intrinsic coagulation pathways were not influenced by these nanocomposites. The possible reason is that a large number of hydroxyl groups were introduced to nanocomposites in the process of preparation,[28] which the resulting hybrids possessed electronegative surface. A nanomaterial with high negative charge (Figure 2B) may be not favorable for platelet aggregation

and the formation of coagulation. Compared with free GO, these MNPs-binding GO nanocomposites are safer, because free GO potentially induced the high thrombosis, or blood clots according to the literature.[21]

4.3 Cytotoxicity and apoptosis assay in vitro

According to the cell viability, uGO@Fe_3O_4 NPs possessed lower growth inhibition activity than uGO@Fe_3O_4 NSs (Figure 5), reflecting that the former showed better cytocompatibility than the latter. This may be attributed to its spherical structure except high negative zeta potential tending to repelling negatively charged cell membrane. The representative HepG2 cells simultaneously appeared green fluorescence cytoplasm and red fluorescence nucleus based on LSCM image (Figure 5C), verifying that the cells have been at a later stage of apoptosis even necrosis. This is because annexin V-FITC can only react with phosphatide acyl serine inside membrane and propidium iodide (PI) can only stain dead cell. Quantitative detection on flow cytometry indicated that uGO@Fe_3O_4 NPs or uGO@Fe_3O_4 NSs can dose-dependently activate apoptosis of HepG2 and L02 cells (Figure 5D), implying that uGO@Fe_3O_4 composites existed certain cytotoxicity. It can be seen that HepG2 and L02 cells treated with uGO@Fe_3O_4 NSs showed 1.6 and 1.5 times apoptotic cell higher than the corresponding cells treated with uGO@Fe_3O_4 NPs under the same conditions, suggesting that uGO@Fe_3O_4 NSs showed higher growth inhibition activity for two kinds of cells compared to uGO@Fe_3O_4 NPs. These data were similar to the results assayed by WST-8 test. The overhang in toxicity may be because cell membrane was damaged through physical interaction with uGO@Fe_3O_4 nanosheets with sharp edges. As described in the previous literature, a graphene nanosheet possessing sharp edges caused considerable damage to the cell membrane of bacteria.[39] Furthermore, Wang et al. declared GO could cause cell apoptosis or death through disturbing the course of cell energy metabolism and gene transcription and translation after entering into cytoplasm by endocytosis pathway.[20] This explanation applies equally well to uGO@Fe_3O_4 nanosheets.

4.4 Body weight change analysis

Although cytotoxicity of GO-based magnetic nanocomposites in vitro have been reported in some scientific literature,[13-15] it is still essential to evaluate the toxicity and biocompatibility in animal. It was observed that 7 days after treated with uGO@Fe_3O_4 NPs or NSs, even 14 days, the Wistar mice did not die and were still in good conditions, reflecting that the nanocomposites have

no acute lethal toxicity within tested doses (5～10 mg Fe/kg). Further research found that there seemed to be discrepancies in body weight change (BWC) among control and two sample groups between the start and the last day (14 day) of treatment (Table 2). BWC in mice treated with uGO@Fe_3O_4 NPs or NSs were significantly smaller than those in the control mice. Especially, the gained weight in NSs group only approximately accounted for 40% of the control. The emaciation can be attributed to exogenous stimuli. However, none of the BWC results for the different dose groups of the same sample are statistically significant in Table 2. These results showed that uGO@Fe_3O_4 NPs or NSs inhibited the growth of the mice and have a physical toxicity to a certain extent, but dosage-dependent effect was inapparent.

Table 2

Body weight change (BWC, g) between the start and the last day (14 day) of treatment to research a physical toxicity caused by uGO@Fe_3O_4 NPs or NSs with 5, 7.5, and 10 mg Fe/kg of dosages. Control group was injected PBS. The data are expressed as mean±S.D. (n=5). *$p<0.05$ versus control according to ANOVA.

Groups	Dosage (mg Fe/kg BW)	BWC (g)
Control	PBS	17.6±5.2
uGO@Fe_3O_4 NPs	5	13.6±2.4
	7.5	14.8±3.6
	10	13.4±3.9
uGO@Fe_3O_4 NSs	5	7.3±1.6*
	7.5	7.1±2.1*
	10	6.8±3.7*

4.5 Blood biochemical assays

In order to further explore toxicity mechanism, eight main blood biochemical indicators were assayed. As shown in Figure 6, the uGO@Fe_3O_4 NPs and NSs induced a severe hepatic injury as evidenced by the significant enhancement of TBIL, ALT, AST, and ALP levels ($p \leqslant 0.05$) and decline of ALB level ($p \leqslant 0.05$). Especially, the high-dosage exposure of uGO@Fe_3O_4 NPs and NSs enhanced the damage on hepatic. Although CREA data there was only small fluctuation, a sharp rise in BUN level (Figure 6F,G) still implied the existence of nephrotoxicity. The significant increase of LDH level in the serum further testified the damage of multiple tissues, such as liver and spleen.

4.6 Biodistribution of GO@MNPs nanocomposites

In vivo studies determining graphene oxide-based magnetic nanocomposites effects upon

organs are scarce in the literature. The present work conducted their biodistribution in mice by iron element measurements and MRI detection. It can be found that the Fe element rapidly distributed in blood, heart, liver, spleen, lung and kidney as the blood flow after GO@MNPs nanocomposites were injected (Figure 7). In the blood, though Fe concentration rose to the peak 1 h after injection, the amplitude of its variation was very small compared to other tissues, suggesting that nanocomposites were fast transported from blood plasma to solid organs. By contrast, even 14 d after injection, the other five tissues treated with uGO@Fe_3O_4 NSs still remained a certain amount of iron elements, demonstrating that the uGO@Fe_3O_4 NSs were not easy to be completely removed from these tissues. Liver and spleen possessed the highest Fe concentration in all detected tissues, and Fe remained constant 14 d after injection, reflecting that a large quantity of nanocomposites was intercepted. This is in agreement with previous research findings.[35,40] Particularly, large dose of uGO@Fe_3O_4 NSs displayed the larger interception both in liver and spleen compared to uGO@Fe_3O_4 NPs, showing that dosage and morphology of nanocomposites are important factors influencing the interception and accumulation. Furthermore, it is possible for exogenous nanosheets with irregular edge to enhance the phagocytosis of macrophages in liver and spleen. These results were confirmed by MR imaging (Figure 8). In these T_2-weighted images, the negative enhancement apparently illustrated that the uGO@Fe_3O_4 NPs/NSs largely accumulated in the reticuloendothelial system (RES), such as liver and spleen. The uGO@Fe_3O_4 NSs had a longer accumulation process compared to uGO@Fe_3O_4 NPs.

4.7 Histopathological analysis

The fact that the uGO@Fe_3O_4 NSs and NPs tended to persistent accumulation in the liver and spleen provided evidence for tissue injury, especially, hepatic injury. Hepatic architecture of normal mice showed regular cell distribution and normal histology without any damage (Figure S2 Control). However, histopathological findings of hepatic tissue of exposure to uGO@Fe_3O_4 NSs revealed serious granulomas (G), swollen vacuolated bundles (S) and interstitial edema (E) (Figure S2(A)). The inflammation sites can be more clearly observed in histological image by only H&E staining without iron Prussian blue staining in the liver (Figure 10). This may be because nanomaterial, such as uGO@Fe_3O_4 NSs with sharp edges, punctured tissue cells. Another possible reason of the organ lesions may be associated with a dispersive mode of GO-based particulate deposition in the liver. At 24 h, or later, macrophage-containing granulomas were

formed. A careful observation could discern that the granulomas main gathered around uGO@Fe_3O_4 NSs. Subsequently, the granulomas further developed into vacuolated bundles and interstitial edema.

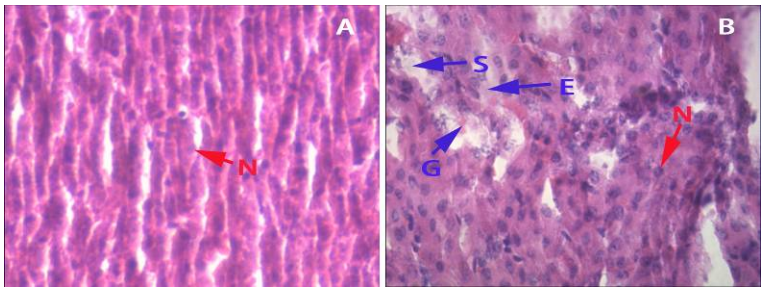

Figure 10. Representative histological images of the liver of (A) control and (B) exposure to uGO@Fe_3O_4 NSs at 7 days. (H&E stain, 40×). Blue particles show cell nuclei (N).

The uGO@Fe_3O_4 NSs and NPs tended to induce tissues injury, which prompts surface modification for graphene or graphene-based magnetic nanocomposite.[22,41-44] Surface coating is very important to control toxicity of nanomaterials. In fact, the surface modifications for graphene-based magnetic nanocomposite with biocompatibility polymer materials, such as chitosan or PEG, are being conducted by us as a continuation of the work.

4.8 Gene expression

Liver tissue is the important site for xenobiotic metabolism. In most cases, the metabolic and detoxification processes are achieved in the liver by activating superoxide dismutase, catalase, and glutathione peroxidase. SOD, CAT, and GPx constitute the primary antioxidant system.[45] These antioxidant enzyme genes are mainly responsible for eliminating superoxide anion radicals by reduction reaction.[46] When liver was damaged, organisms activated antioxidant defense passages to inhibit reactive oxygen species (ROS) generation.[47] Interestingly, in present study, three genes manifested rather different expression patterns under the same dose. The findings confirm that uGO@Fe_3O_4 NPs and NSs suppressed mRNA expression levels of SOD and upregulated mRNA expression levels of GPx, while the effect on CAT gene expression changed with dose. This pattern reflected GPx in antioxidant system was preferentially activated during the uGO@Fe_3O_4 nanocomposite exposure. Only when exposed to high doses of uGO@Fe_3O_4 NPs or NSs (10 mg Fe/kg), did organisms increase CAT gene expression level. Enhancement of CAT and GPx expression may imply that there was more generation of ROS in cells after exposure to nanomaterials. CAT and GPx were broadly studied in other species. For example, rat expressing

CAT and GPx in liver tissue resisted lead-induced oxidative stress.[48] The previous literature reported that the toxicity mechanism of the exogenous substances is associated with the turbulence in the oxidative stress-antioxidant balance.[49] It is worth noting that over expression of the CAT and GPx at high doses may induce premature senescence, in turn, affect growth and development, as mentioned emaciation above. With regard to the decrease in SOD mRNA expression, we deduce the weakening of the metabolic capacity of the mouse. According to the literature,[50] organism will reduce appropriate metabolic functions in the case of extreme oxidative stress.

5. Summary

This study evaluated the safety of ultrafine graphene oxide-based magnetic NPs and NSs *in vitro* and *in vivo*. The data *in vitro* suggest that uGO@Fe_3O_4 NSs showed higher growth inhibition activity for HepG2 cells and L02 cells, and induced higher hemolysis than uGO@Fe_3O_4 NPs. Although intrinsic coagulation values did not break through the normal range at all tested concentrations, the nanomaterials at high concentration caused extrinsic coagulation. After intravenous injection, the accumulation in mice mainly occurred in reticuloendothelial system and increased with dosage and exposure time. A long time deposition in tissues induced granulomas, subsequently, further developed into vacuolated bundles and interstitial edema. The significant fluctuation of blood biochemical indicators testified that the uGO@Fe_3O_4 NPs and NSs induced a severe hepatic injury. Enhancement of CAT and GPx expression further demonstrated that there was more generation of ROS in liver due to hepatic injury after exposure to nanomaterials. Therefore, uGO@Fe_3O_4 NPs and NSs are the initial factors of toxicity.

Conflict of interest

The authors have declared that there is no conflict of interest.

Acknowledgments

This study was supported by the Talents Fund for Basic Disciplines of National Science Fundation of China (J1210077, J1210033, J1103502) and the basic scientific research business expenses of the central university and open project of key laboratory for magnetism and magnetic materials of the ministry of education, Lanzhou University (no. LZUMMM2012006).

Notes

[a] Department of Biochemistry and Molecular Biology, School of Life Sciences, Lanzhou University, Lanzhou, Gansu 730000, China

[b] The People's Hospital of Gansu Province, Lanzhou, Gansu 730000, China

* Corresponding author, Fax: +86-931-891-5208; Tel: +86-15117266908.

E-mail: shenjianmin@lzu.edu.cn (Jianmin Shen)

References

1 J. C. Li, Y. He, W. J. Sun, Y. Luo, H. D. Cai, Y. Q. Pan, M. W. Shen, J. D. Xia and X. Y. Shi, Biomaterials, 2014, 35, 3666-3677.
2 J. R. McCarthy and R. Weissleder, Adv. Drug Deliver. Rev., 2008, 60,1241–1251.
3 S. Laurent, S. Dutz, U. O. Häfeli and M. Mahmoudi, Adv. Colloid. Interfac., 2011, 166, 8–23.
4 L. Z. Bai, D. L. Zhao, Y. Xu, J. M. Zhang, Y. L. Gao, L. Y. Zhao and J. T. Tang, Mater. Lett., 2012, 68, 399–401.
5 V. I. Shubayev, T. R. Pisanic and S. H. Jin, Adv. Drug Deliver. Rev., 2009, 61, 467–477.
6 A. J. Cole, A. E. David, J. X. Wang, C. J. Galbán, H. L. Hill and V. C. Yang, Biomaterials, 2011, 32, 2183-2193.
7 M. M. Yallapu, S. F. Othman, E. T. Curtis, B. K. Gupta, M. Jaggi and S. C. Chauhan, Biomaterials, 2011, 32,1890-1905.
8 K. S. Novoselov, Z. Jiang, Y. Zhang, S. Morozov, H. Stormer, U. Zeitler, J. Maan, G. Boebinger, P. Kim and A. Geim, Science, 2007, 315,1379.
9 A. A. Balandin, S. Ghosh, W. Bao, I. Calizo, D. Teweldebrhan, F. Miao and C. N. Lau, Nano Lett., 2008, 8, 902–907.
10 C. Lee, X. Wei, J. W. Kysar and J. Hone, Science, 2008, 321, 385.
11 J. G., Liu, L. Cui and D. Losic, Acta Biomaterialia, 2013, 9, 9243–9257.
12 G. S. Wang, G. Y. Chen, Z. Y. Wei, X. F. Dong and M. Qi, Mater. Chem. Phys., 2013, 141, 997-1004.
13 L. Yan, Y. N. Chang, L. N. Zhao, Z. J. Gu, X. X. Liu, G. Tian, L. J. Zhou, W. L. Ren, S. Jin, W. Y. Yin, H. Q. Chang, G. M. Xing, X. F. Gao and Y. L.Zhao, Carbon, 2013, 57,120-129.
14 W. H. Chen, P. W. Yi, Y. Zhang, L. M. Zhang, Z. W. Deng and Z. J. Zhang, ACS Appl. Mater. Inter., 2011, 3, 4085–4091.
15 X. X. Ma, H. Q. Tao, K. Yang, L. Z. Feng, L. Cheng, X. Z. Shi, Y. G. Li, L. Guo and Z. Liu, Nano Res., 2012, 5, 199–212.
16 A. B. Seabra, A. J. Paula, R. d. Lima, O. L. Alves and N. Duran, Chem. Res. Toxicol., 2014, 27, 159−168.
17 Y. Chang, S. T. Yang, J. H. Liu, E. Dong, Y. Wang, A. Cao, Y. Liu and H. Wang, Toxicol. Lett., 2011, 200, 201-210.
18 T. Lammel, P. Boisseaux, M. L. Fernández-Cruz and J. M. Navas, Part. Fibre Toxicol., 2013,10, 27.
19 J. Yuan, H. C. Gao, J. J. Sui, H. W. Duan, W. N. Chen and C. B. Ching, Toxicol. Sci., 2012, 126, 149-161.
20 K. Wang, J. Ruan, H. Song, J. L. Zhang, Y. Wo, S. W. Guo and D. X. Cui, Nanoscale Res. Lett., 2011, 6, 8-15.
21 S. K. Singh, M. K. Singh, P. P. Kulkarni, V. K. Sonkar, J. J. A. Gracio and D. Dash, ACS Nano, 2012, 6, 2731–2740.
22 K. Yang, S. Zhang, G. X. Zhang, X. M. Sun, S.T. Lee and Z. Liu, Nano Lett., 2010, 10,

3318–3323.
23 T.S. Hauck, R. E. Anderson, H. C. Fischer, S. Newbigging and W. C. W. Chan, Small, 2010, 6,138–144.
24 C. F. Jones and D. W. Grainger, Adv. Drug Deliver. Rev., 2009, 61(6), 438-456.
25 R. F. Phalen, M. J. Oldham and A. E. Nel, Toxicol. Sci., 2006, 92, 126–132.
26 C. Y. Wang, S. Ravi, U. S. Garapati, M. Das, M. Howell, J. Mallela, S. Alwarappan, S. S. Mohapatra and S. Mohapatra, J. Mater. Chem. B, 2013, 1, 4396–4405.
27 L. Ai, C. Zhang and Z. Chen, J. Hazard. Mater., 2011, 192,1515–1524.
28 J. M. Shen, F. Y. Gao, L. P. Guan, W. Su, Y. J. Yang, Q. R. Li and Z. C. Jin, RSC Adv., 2014, 4, 18473–18484.
29 R. S. Yang, L. W. Chang, J. P. Wu, M. H. Tsai, H. J. Wang, Y. C. Kuo, T. K. Yeh, C. S. Yang and P. Lin, Environ. Health Persp, 2007, 115, 1339–1343.
30 A. A. Attia, R. H. El-Mazoudy and N. S. El-Shenawy, Pestic. Biochem. Phys., 2012, 103, 87–93.
31 Y. S. Lin and C. L. Haynes, J. Am. Chem. Soc., 2010, 132, 4834–4842.
32 Y. N. Sun, C. D. Wang, X. M. Zhang, L. Ren and X. H. Tian, J. Nanosci. Nanotechno., 2011, 11, 1210-1216.
33 C. L. Yang, S. J. Huang, C. W. Chou, Y. C. Chiou, K. P. Lin, M. S. Tsai and K. C. Young, Talanta, 2013, 116, 704–711.
34 H. X. Wu, S. J. Zhang, J. M. Zhang, G. Liu, J. L. Shi, L. X. Zhang, X. Z. Cui, M. L. Ruan, Q. J. He and W. B. Bu, Adv. Funct. Mater., 2011, 21, 1850–1862.
35 R. Y. Hong, B. Feng, L. L. Chen, G. H. Liu, H. Z. Li, Y. Zheng and D. G. Wei, Biochem. Eng. J., 2008, 42,290–300.
36 K. H. Liao, Y. S. Lin, C. W. Macosko and C. L. Haynes, ACS Appl. Mater. Inter., 2011, 3, 2607–2615.
37 J. Chen, X. Wang and H. Han, J. Nanopart. Res., 2013, 15, 1658−1671.
38 C. H. Shih, C. H. Lu, J. H. Wu, C. H. Lin, J. M. Wang and C. Y. Lin, Sensor. Actuat. B-Chem., 2012,161, 1184–1190.
39 O. Akhavan and E. Ghaderi, ACS Nano, 2010,4, 5731−5736.
40 L. Gu, R. H. Fang, M. J. Sailor and J. H. Park, ACS Nano, 2012,6, 4947-4954.
41 K. Yang, J. M. Wan, S. Zhang, Y. Zhang, S.T. Lee and Z. Liu, ACS Nano, 2011, 5(1), 516-522.
42 S. Zhang, K. Yang, L. Z. Feng and Z. Liu, Carbon, 2011,49(12), 4040-4049.
43 K. Yang, L. L. Hu, X. X. Ma, S. Q. Ye, L. Cheng, X. Z. Shi, C. H. Li, Y. G. Li and Z. Liu, Adv. Mater. 2012, 24, 1868–1872.
44 X. Z. Shi, H. Gong, Y. J. Li, C. Wang, L. Cheng and Z. Liu, 2013, 34(20), 4786-4793.
45 M. Hajiani, F. Razi, A. Golestani, M. Frouzandeh, A.A. Owji, S. Khaghani, N. Ghannadian, A. Shariftabrizi and P. Pasalar, Redox. Rep., 2012, 17,101–107.
46 J. S. Seo, Y. M. Lee, H. G. Park and J. S. Lee, Biochem. Biophys. Res. Commun., 2006, 340, 901–908.
47 J. S. Rhee, R. O. Kim, H. G. Choi, J. Lee, Y. M. Lee and J. S. Lee, Comp. Biochem. Physiol. C: Toxicol. Pharmacol., 2011, 154, 19–27.
48 C. M. Liu, Y. L. Zheng, J. Lu, Z. F. Zhang, S. H. Fan, D. M. Wu and J. Q. Ma, Environ. Toxicol. Phar., 2010,29, 158–166.

49 A. O. Abolaji, J. P. Kamdem, T. H. Lugokenski, T. K. Nascimento, E. P. Waczuk, E. O. Farombi, É. L. S. Loreto and J. B. T. Rocha, Free Radical. Bio. Med., 2014, 71, 99-108.

50 J. F. Zhang, X. R. Wang, H. Y. Guo, J. C. Wu and Y. Q. Xue, Ecotoxicol. Environ. Saf., 2004, 58, 110–116.